Contact Sensing via Active Oscillatory Actuation

Rahul Mitra*, Kirkland Boyd*, Divas Subedi*, Digesh Chitrakar*, Edwin Aldrich*,
Ananya Swamy*, and Kevin Huang*
*Department of Engineering, Trinity College, Hartford Connecticut, USA
Email: {rahul.mitra, kirkland.boyd, divas.subedi, digesh.chitrakar,
edwin.aldrich, ananya.swamy, kevin.huang}@trincoll.edu

***Abstract*—Collaborative robotic approaches seek to incorporate either direct human intervention in tasks previously suited for isolated robot devices, or to use precise machines (cobots) to assist in sensitive tasks. Cobots work alongside humans to extend the scope of robot assistance to spaces such as service and dynamic industrial or assembly tasks. With that said, the close proximity of humans with machines necessitates safe interaction, which can be achieved via lightweight materials and novel sensing capabilities. The inherent physical strength needed in some robot tasks, such as in assembly, make contact sensing of particular concern when introducing a human collaborator. A minimally intrusive method that can be seamlessly subsumed into extant devices is desired. In this paper, such a contact sensor is prototyped and tested. The sensor is bidirectional in that it actively provides an oscillatory actuation signal to a rigid link while simultaneously recording and analyzing the mechanical vibration of said link. Natural oscillation frequency shifts and energy concentration changes due to damping are congruent with different types of contact with the rigid link. The method is lightweight, low-cost and can be quickly incorporated into various manipulators. The developed configuration is advantageous as it does not require any delicate sensors on the robot body and relies primarily on actuated oscillations of the manipulator. Oscillatory acceleration data is collected and subsequently used to train and classify different contact locations using frequency-based features. Three separate classes are distinguished according to contact location. Results are promising and show excellent classification of both contact and contact location.**

***Keywords* — active sensing, sensors, collaborative robots, collision detection, machine learning**

I. Introduction

Sensors have been developed to enable a sense of touch for machines. Previous works have extracted information about the roughness, temperature, and stiffness of an object [1] through tactile sensing. Some applications of touch sensing in robotics include prosthetics, orthotics and robot-assisted minimally invasive surgery (RMIS) [2]–[6]. While kinematic joint torque sensors can be used to approximate end-effector force, sensing and localising minor contacts are remaining challenges. Furthermore, serial linkages accumulate error. A low-cost, seamless end-effector contact sensor is desired.

Backus et al. introduced a binary touch sensor tracking a digit's resonant frequency [7], [8]. Despite the robustness of the sensor, the method was both involved and intrusive. The work presented here is motivated to resolve this limitation and aims to investigate the localisation of various contact points based on shifts in damped natural frequency of an actively vibrated link. Current robotic manipulators use visual and force servoing to perform predefined motor tasks, while proximity sensing oftentimes utilizes an array of sensors (capaciflextive, infrared, or ultrasonic) constantly evaluating data [9]–[11]. The prototype in this work is based off of the work of Backus et al., for which an inexpensive contact sensor is constructed for contact detection. Minute contact detection and localization is of interest when handling delicate or valuable structures or for observing states in tasks like locomotion. In this system, a steel rod is fixed to an actuated eccentric rotating mass motor (ERM) as depicted in Fig 1. The repeatable contact mechanism is implemented using a precision servo.

The primary objective of the study was to empirically classify the contact points on the vibrating rod based on natural oscillation frequencies and energies. This paper proposes a design for a simple sensor for localizing contacts made with low-cost components with minimal intrusiveness compared to prior art. The overall workflow is shown in Fig. 2

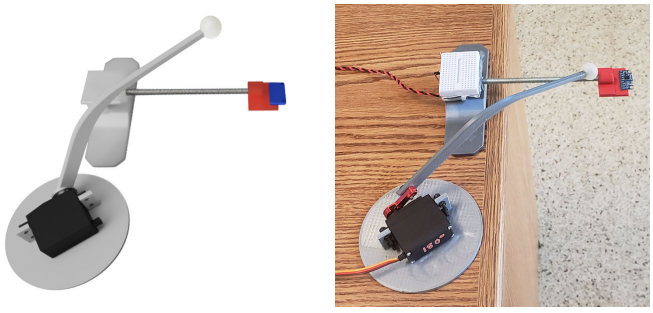

(a) (b)

Figure 1: Physical test setup; actuated rigid link, accelerometer sensor at terminal end (red), and contact probe. (a) CAD rendering untouched; (b) real-world setup contact.

A. Contributions

To the best of the authors' knowledge, this work is the first:

i) to empirically classify contact locations on an actively oscillating rigid link for contact detection and localization based on transient oscillatory response and;
ii) to implement a low-cost and low-intrusion method for augmenting rigid links with contact sensing capabilities.

Although the proposed design is not optimized for the actuation signal, the platform demonstrates the flexibility of the approach to arbitrary robotic links. The study also prompts future research in this area and perhaps other sensing modalities.

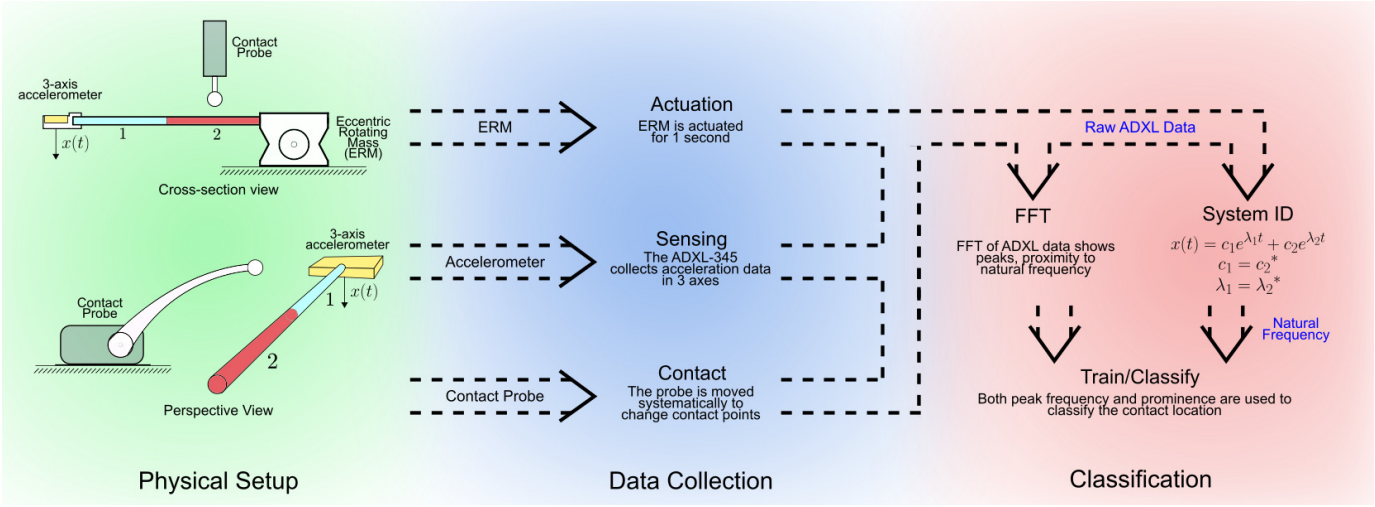

Figure 2: In Physical Setup, the rigid link is actuated with an eccentric rotating mass (ERM) motor, while simultaneously an ADXL 3-axis accelerometer measures acceleration at the terminal end of the link. Contacts are applied via a contact probe at two different regions. In Data Collection, pulsed actuation as well as simultaneous recordings are conducted while systematically collecting data from the two contact regions and the untouched case. Measurements are used for system identification assuming a linear time-invariant second order system. The data are parsed into feature-space and classified.

II. Related Work

A. Accelerometer-based Robot State Observation

Quigley et al. [12] introduced a method for estimating the kinetic configuration of a robotic manipulator. This setup used a low-cost 3D micro-electromechanical system (MEMS) accelerometer at each joint in the robotic serial link mechanism. Joint states were estimated using an Extended Kalman Filter (EKF) with updates based on accelerometer data. Because of its low cost, this method can be used to augment existing robotic systems by simply adding accelerometers to mechanical joints. Similarly, Weiser et al. [13] implemented an estimated robot kinematic state using priors measured by initial input and the gravity vector measured by triaxial accelerometers. Low-cost accelerometers can be used successfully to obtain kinematic state, and can be used in concert at each link or joint.

B. Contact Localization

McMahan et al. [14] used an array of multiple MEMS accelerometers to localize contact events along a robotic manipulator. This sensing arrangement enabled the system to distinguish between desired and undesired contact events that occurred at its surface via supervised learning methods. In particular, a support vector machine (SVM) was used to train a classifier to identify and categorize contact events [15].

C. Machinery Fault Diagnosis

Vibrational analysis using frequency spectrum data can provide insight into diagnosing mechanical faults in machinery. Li et al. presented a motor rolling bearing fault diagnosis approach using neural networks and time/frequency domain bearing vibration analysis [16]. Signals from vibration sensors are usually measured and compared with reference measurements in order to determine and interpret system conditions [16]. Examples of methods used to interpret signals for mechanical fault diagnosis include probabilistic analysis [17], frequency analysis [18]–[20], time-domain analysis [21] and finite-element analysis [22]. Of the presented methods, the frequency analysis method is most popular. The Fourier transform method [23] allows for the analysis of the signal in the frequency domain (as opposed to the time domain) where characteristics of the signal may be more easily noticed. In this work, Fourier analysis is used to interpret and distinguish signals from an undisturbed link versus one in contact.

D. Residual Vibration Analysis and Suppression in Industrial Robotics

Industrial robots require fast and precise motions in order to achieve desired effectiveness and productivity [24]. Robots undergo a series of motions resulting in accelerating to operational velocities and then again decelerating to a complete stop [25]. These motions, however, lead to residual vibrations that tend to be time-varying and non-linear due to configuration-dependent friction, inertia variation and non-linear stiffness of joints [24]. Singer et al. presented a method for the suppression of residual vibrations of one degree-of-freedom (DOF) of a 6 DOF robot by implementing an Input Shaping Technique (IST) [26]. However, the IST was only effective on linear time invariant systems. Practically all industrial robotic systems exhibit time-varying and non-linear residual vibrations [24]. As such, Park et al. modified the current model of IST to an Iterative Learning Input Shaping Technique (LIST) [24] so as to achieve applicability in industrial systems. Tao et al. used a mathematical model based on kinetic energies leading to Lagrangian equations to analyze and suppress residual vibrations in the Selectively Compliant Articulated Robot Arm (SCARA) robots for wafer handling [25].

III. Methods

The overall system workflow is depicted in Fig. 2. The procedural methodology for this research consisted of three components:

A. System Hardware Components;
B. Experimental Data Collection;
C. Data Analysis - Feature Extraction and Classification

detailed in the following subsections.

A. System Hardware

The rigid link utilized in this work consisted of a ¼ inch UNC 20 threaded rod of ASTM A591 Zinc Coated Steel. The contact probe was composed of a 3D printed PLA plastic arm and an ultra-strength silicone ⅝ inch rubber ball. Affixed to the terminal end of the threaded rod was a low-cost ADXL 3-axis accelerometer (sampling frequency of 3200 Hz) with a 3D printed PLA plastic mount. The contact probe arm was actuated with a standard precision MG995 metal gear servo, and precise contacts were placed at either of the two contact regions as shown in Fig. 2.

B. Experimental Data Collection

Data were collected automatically with 200 samples drawn from each of the following three classes:

i) untouched;
ii) contact at Region 1;
iii) contact at Region 2.

Samples were collected in three blocks of 200 – one block per class. The untouched case implies that no contact was applied to the rigid link, as the steel rod was fixed only at one end. As depicted in Fig. 2, two different contact regions were examined, labeled Region 1 and Region 2. Region 1 entailed contact in the terminal half of the rigid link, while Region 2 contacts consisted of ones in the proximal half.

As described in detail in Section III-C1, the transient oscillatory response of the rigid link is of interest. Thus, the experimental data collection began with the mechanical system at rest. To initiate a sample, the contact probe was positioned via the servo mechanism for the corresponding data type (untouched, Region 1, or Region 2). The ERM was then actuated with a constant supplied voltage for precisely one second, during which time sensor data was also collected. The mechanical and electrical system was then allowed to return to rest state as zero voltage was applied to the ERM for 180 seconds. This process was repeated to collect the entire database of 600 time series samples.

C. Data Analysis - Feature Extraction and Classification

After data were collected, two separate post-processing modules were used to construct the classifier. The first module performed system identification, providing *a priori* information for the classifier. The second module classified the data based on both raw data and results from the first module.

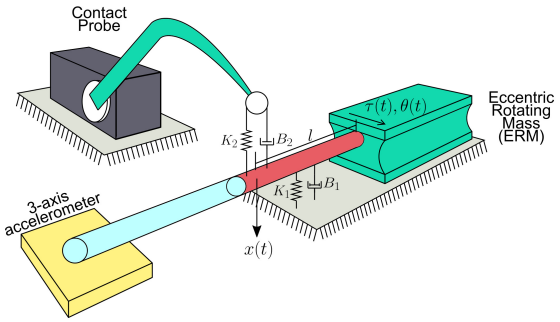

(a) Second order perspective drawing of sensor overlaid with system components.

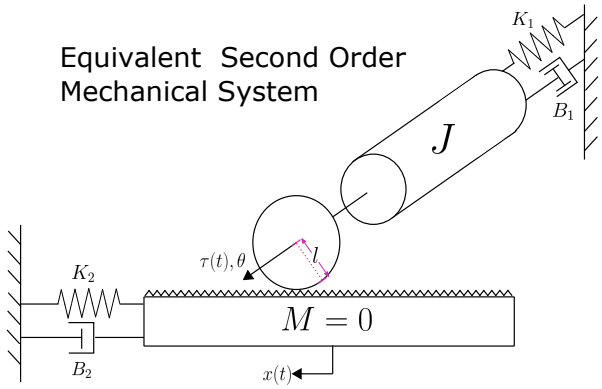

(b) Equivalent second order model – broken down into rotational and translational system components.

Figure 3: Second order mechanical systems representing the dynamics of the sensor.

1) System Identification: For this prototype, the vibrating rigid link in contact was assumed to behave as a second order rotational-translational mechanical system. The relevant parameters and physical setup are shown in Fig. 3.

With small angle approximation, i.e. $\sin(\theta) \approx \theta$ for small θ, the translational components are converted to rotational and vice versa via

$$x(t) = \theta(t) l \tag{1}$$

For untouched with an input torque applied at the proximal end of the rigid link, the behavior is purely rotational and is governed by the following linear second order differential equation

$$J\frac{d^2\theta}{dt^2} + B_1\frac{d\theta}{dt} + K_1\theta(t) \quad = \tau\,(t) \tag{2}$$

where J, B_1 and K_1 are the inertia, damping coefficient and spring constant of the untouched rigid link respectively. When in contact, translational system elements from the contact probe are introduced, and the governing equation extends to

$$J\frac{d^2\theta}{dt^2} + B_1\frac{d\theta}{dt} + K_1\theta(t) \quad = \tau(t) - \tau_p(t) \tag{3}$$

where $\tau_p(t)$ is a counter-acting torque applied by the contact probe. This torque is defined as $\tau_p(t) = l \times f(t)$ where

$$B_2\frac{dx}{dt} + K_2 x(t) = f(t) \tag{4}$$

Applying (1) and its time derivatives to (4), the second order model for the sensor in contact is derived as

$$\frac{d^2\theta}{dt}+\left(\frac{B_1+B_2l^2}{J}\right)\frac{d\theta}{dt}+\left(\frac{K_1+K_2l^2}{J}\right)\theta(t)=\frac{1}{J}\tau(t) \quad (5)$$

The canonical second order system

$$\frac{1}{\omega_n^2}\frac{d^2\theta}{dt}+2\frac{\zeta}{\omega_n}\frac{d\theta}{dt}+\theta(t)=0$$

was used to inform approximate physical parameters based on measured natural frequency, ω_n, and damping ratio, ζ.

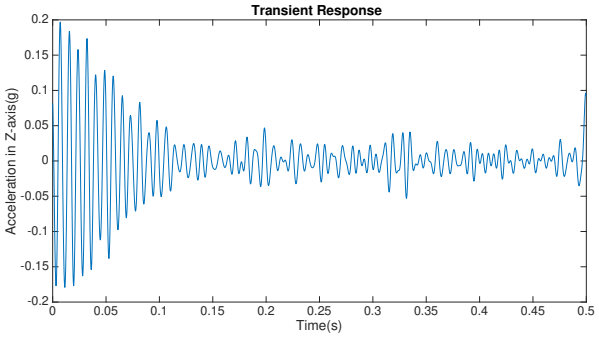

Figure 4: Sample oscillatory transient response.

ω_n and ζ were derived empirically from the oscillatory transient response, with homogeneous response of

$$\theta(t)=c_1e^{\lambda_1 t}+c_2e^{\lambda_2 t}$$

where

$$\omega_n=||\lambda_1||_2=||\lambda_2||_2$$

ω_n was ascertained from the transient response and used to elicit the damped natural frequency ω_d, as depicted in Fig. 4

Based on preliminary measurements and system identification, damped natural oscillatory frequencies between 0 and 100 Hz are expected for the rigid link in contact. Note that (1) and (4) allow the assumption that the accelerometer measurements should behave as $\theta(t)$ and its time derivatives.

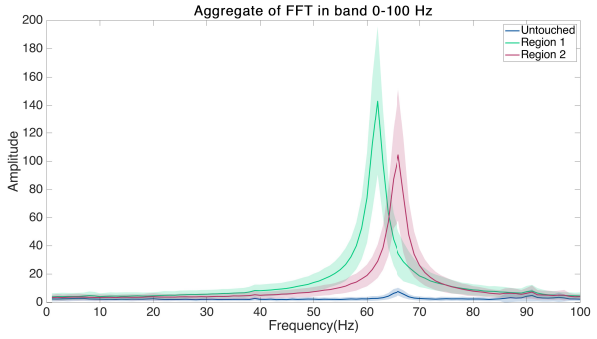

Figure 5: Aggregate FFTs from the three classes. From this, it is clear that the untouched case exhibits very little energy in the 0-100 Hz band, while energy is concentrated in narrow bands for contact in Region 1 and Region 2.

2) Classification: The data-set was uniformly segmented within the three classes into a split of 70% training data and 30% test data. All data were first converted to the frequency domain via fast Fourier transformations (FFT). The aggregate FFTs from the three classes with single standard deviation confidence intervals are depicted in Fig. 5. A two-dimensional feature space was thus selected with features as

a) peak prominence, p
b) peak frequency, ω

where peak prominence, p, is defined as the peak value minus either the left or right trough value, whichever is greater. Prior to classification, the data were pre-processed and normalized along both feature dimensions via Z-score normalization. The normalized training data are illustrated in Fig. 6.

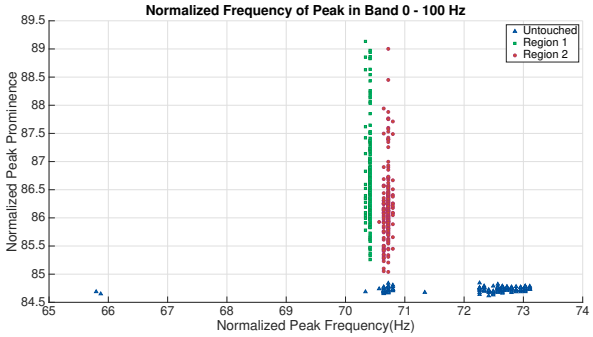

Figure 6: Labeled training data displayed in the Z-score normalized feature space. Note: means are not shifted to zero in this figure for illustration purposes.

a) Gaussian Mixture Model Clustering: Expectation-maximization (EM) clustering was performed to segment the three different classes. The three clusters and probability density functions (PDF) are depicted in Fig. 7.

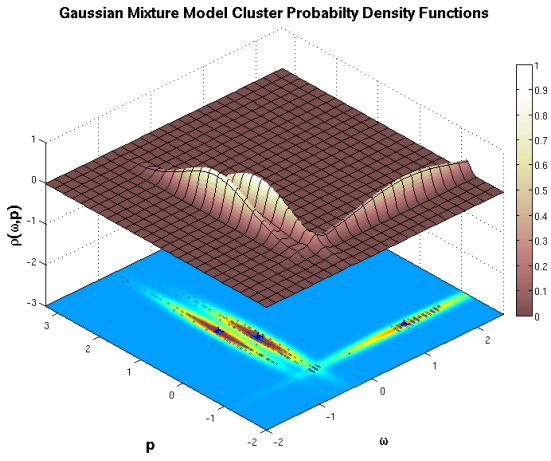

Figure 7: EM clusters PDFs from normalized training set. The color scale is for the three-dimensional PDF surface. On the two-dimensional heat map, centroids are labeled as + and normalized training data as ○.

b) Logistic Regression: A two-stage supervised logistic regression classifier was trained via standard least mean square error. The first stage aimed to separate touched from untouched samples, and the results are shown in Fig. 8.

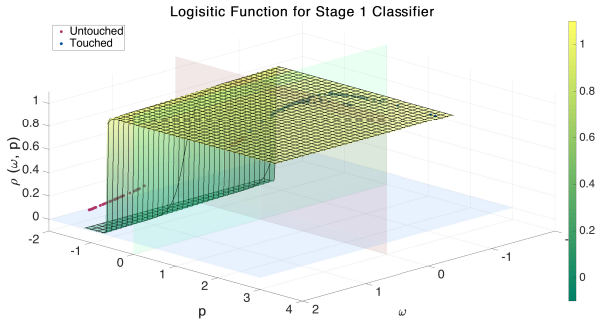

Figure 8: Decision boundary for first stage logistic regression. This classifier distinguishes data corresponding to touched vs. untouched.

Data that were classified as touched were then forwarded to the second stage to classify between touches in Region 1 and Region 2. The second stage regression results are illustrated in Fig. 9.

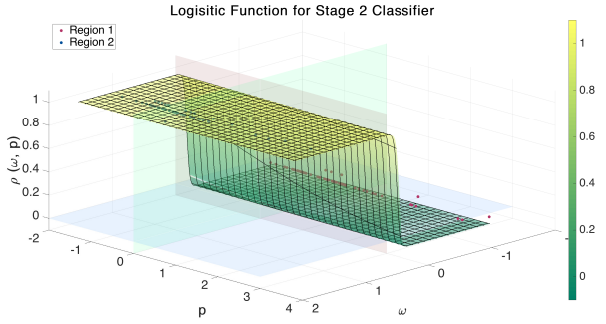

Figure 9: Second-stage logistic regression classifier decision boundary to distinguish touched samples as either Region 1 or Region 2.

IV. Results

A. Distribution of Raw Data

The labeled raw data were also briefly analyzed in one-dimension; peak frequency ω. The distribution of ω for the labeled data are shown in Table I.

Table I: Peak Frequency ω of Rigid Link

Class	Mean ω [Hz]	Standard Dev. [Hz]	Median ω [Hz]
Untouched	85.64	13.4	91.0
Region 1	61.91	0.29	62.0
Region 2	65.80	0.58	66.0

B. EM Classification

Receiver operator curves (ROC) were produced for each of the three classes using the EM unsupervised classifier on the testing data (30% of dataset) and are shown below in Fig. 10. The analyzed threshold was classification probability based on gaussian mixture cluster distributions.

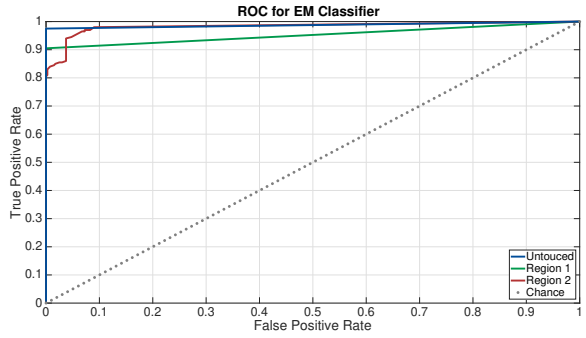

Figure 10: ROC curves from EM unsupervised classifier.

The area under the curve (AUC) for each class was calculated and is tabulated below in Table II.

Table II: AUCs for EM Classifier

Class	Untouched	Region 1	Region 2
AUC	0.9875	0.9525	0.9830

C. Logistic Regression

The first stage logistic decision boundary was trained as

$$\text{logit}(p_t) = \beta_{t0} + \beta_{t1}\omega + \beta_{t2}p \tag{6}$$

where $(\beta_{t0}, \beta_{t1}, \beta_{t2}) = (268.7090, -27.0625, 314.5166)$ and p_t is the probability that a sample, (ω, p), belongs to the touched class. The second stage logistic decision boundary was trained as

$$\text{logit}(p_r) = \beta_{r0} + \beta_{r1}\omega + \beta_{r2}p \tag{7}$$

where $(\beta_{r0}, \beta_{r1}, \beta_{r2}) = (-7.529, 109.6963, -1.3748)$ and p_r is the probability that a sample belongs to the Region 1 class. This two-staged logistic regression classifier was evaluated using the 180 test samples. Precision, recall and accuracy were evaluated for the classifier, and are tabulated in Table III.

Table III: Regression Classification Performance

Class	Precision	Recall	Accuracy
Untouched	1.0	1.0	1.0
Region 1	1.0	1.0	1.0
Region 2	1.0	1.0	1.0

The supervised logistic regression classifier was also evaluated via 10-fold cross validation using 90% training 10% test split. These tests resulted in confusion matrix shown in Fig. 11.

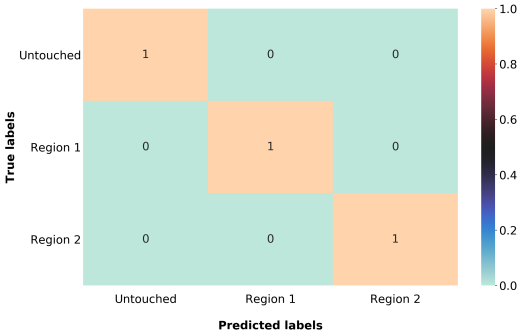

Figure 11: Confusion matrix of logistic regression classifier.

V. Conclusion

This paper presents a novel low-cost method of classifying touch locations for arbitrary single link rigid bodies with minimal augmentation; the only additions were a single ERM and accelerometer. This is in contrast to prior art, which required invasive modifications, arrays of sensors, or well known dynamics of the entire mechanism. The results of this introductory experiment show that contact results in clear energy concentration in the 0-100 Hz band (demonstrated in Table I and Fig. 5) and can be used to distinguish from untouched cases. The damped natural frequency in contact is modified as in (5), which informs contact localization. These observed dynamic behaviors were used to classify untouched, contact in Region 1 and contact in Region 2 using both unsupervised and supervised learning methods: Gaussian mixture model and two-staged logistic regression model respectively. The Gaussian mixture model performed well with AUC scores all above 0.95, as shown in Table II. The supervised logistic model resulted in a perfect classifier, as shown in Fig. 11. These results indicate that the proposed technique is a precise and accurate method to both classify and localize contact. Perfect classification results can be attributed to both low granularity in contact location and high precision in contact probe actuation. Real-world application will require tolerance to variability and incorporate onset detection. To explore the robustness of the technique, future work will explore more divisions of contact location, increased variability in contact actuation, and varying applied force for contact.

Acknowledgements

This work was supported by the Trinity College Summer Research Program. The authors would like to thank Andrew Pace from the University of Washington for technical guidance and feedback.

References

[1] L. Zou, C. Ge, Z. J. Wang, E. Cretu, and X. Li, "Novel tactile sensor technology and smart tactile sensing systems: A review," *Sensors*, vol. 17, no. 11, p. 2653, 2017.

[2] M. I. Tiwana, S. J. Redmond, and N. H. Lovell, "A review of tactile sensing technologies with applications in biomedical engineering," *Sensors and Actuators A: physical*, vol. 179, pp. 17–31, 2012.

[3] K. Huang, D. Chitrakar, R. Mitra, D. Subedi, and Y.-H. Su, "Characterizing limits of vision-based force feedback in simulated surgical tool-tissue interaction," in *2020 43rd Annual International Conference of the IEEE Engineering in Medicine and Biology Society*. IEEE, 2020.

[4] Y.-H. Su, I. Huang, K. Huang, and B. Hannaford, "Comparison of 3d surgical tool segmentation procedures with robot kinematics prior," in *2018 IEEE/RSJ International Conference on Intelligent Robots and Systems (IROS)*. IEEE, 2018, pp. 4411–4418.

[5] Y.-H. Su, K. Huang, and B. Hannaford, "Multicamera 3d reconstruction of dynamic surgical cavities: Non-rigid registration and point classification," in *2019 IEEE/RSJ International Conference on Intelligent Robots and Systems (IROS)*. IEEE, 2019, pp. 7911–7918.

[6] ——, "Real-time vision-based surgical tool segmentation with robot kinematics prior," in *2018 International Symposium on Medical Robotics (ISMR)*. IEEE, 2018, pp. 1–6.

[7] S. B. Backus and A. M. Dollar, "Robust, inexpensive resonant frequency based contact detection for robotic manipulators," in *2012 IEEE International Conference on Robotics and Automation*, 2012, pp. 1514–1519.

[8] ——, "Robust resonant frequency-based contact detection with applications in robotic reaching and grasping," *IEEE/ASME Transactions on Mechatronics*, vol. 19, no. 5, pp. 1552–1561, 2014.

[9] M. R. Cutkosky and W. Provancher, *Force and Tactile Sensing*. Cham: Springer International Publishing, 2016, pp. 717–736.

[10] K. Huang, P. Lancaster, J. R. Smith, and H. J. Chizeck, "Visionless tele-exploration of 3d moving objects," in *2018 IEEE International Conference on Robotics and Biomimetics (ROBIO)*. IEEE, 2018, pp. 2238–2244.

[11] K. Huang, L.-T. Jiang, J. R. Smith, and H. J. Chizeck, "Sensor-aided teleoperated grasping of transparent objects," in *2015 IEEE International Conference on Robotics and Automation (ICRA)*. IEEE, 2015, pp. 4953–4959.

[12] M. Quigley, R. Brewer, S. P. Soundararaj, V. Pradeep, Q. Le, and A. Y. Ng, "Low-cost accelerometers for robotic manipulator perception," in *2010 IEEE/RSJ International Conference on Intelligent Robots and Systems*, 2010, pp. 6168–6174.

[13] E. Wieser, P. Mittendorfer, and G. Cheng, "Accelerometer based robotic joint orientation estimation," in *2011 11th IEEE-RAS International Conference on Humanoid Robots*, 2011, pp. 67–74.

[14] W. McMahan, J. M. Romano, and K. J. Kuchenbecker, "Using accelerometers to localize tactile contact events on a robot arm," in *Proceedings of Workshop on Advances in Tactile Sensing and Touch-Based Human-Robot Interaction, ACM/IEEE International Conference on Human-Robot Interaction*. Citeseer, 2012.

[15] H. Yu and S. Kim, "Svm tutorial-classification, regression and ranking." *Handbook of Natural computing*, vol. 1, pp. 479–506, 2012.

[16] B. Li, M.-Y. Chow, Y. Tipsuwan, and J. C. Hung, "Neural-network-based motor rolling bearing fault diagnosis," *IEEE transactions on industrial electronics*, vol. 47, no. 5, pp. 1060–1069, 2000.

[17] G. Lipovszky, K. Sólyomvári, and G. Varga, *Vibration testing of machines and their maintenance*. Elsevier Science Ltd, 1990, vol. 10.

[18] T. A. Harris, *Rolling bearing analysis*. John Wiley and sons, 2001.

[19] H. Ohta and N. Sugimoto, "Vibration characteristics of tapered roller bearings," *Journal of Sound and vibration*, vol. 190, no. 2, pp. 137–147, 1996.

[20] P. Eschmann, *Ball and roller bearings: Their theory, design, and application*. Heyden, 1958.

[21] K. M. Ragulskis, A. Y. Yurkauskas, and E. I. Rivin, *Vibration of Bearings*. CRC Press, 1989.

[22] M. Donley, W. Stokes, G. Jeong, J. Suh, and S. Jung, "Validation of finite element models for noise/vibration/harshness simulation," *Sound and Vibration*, vol. 30, no. 8, pp. 18–23, 1996.

[23] J. B. Marion, *Classical dynamics of particles and systems*. Academic Press, 2013.

[24] J. Park, P.-H. Chang, H.-S. Park, and E. Lee, "Design of learning input shaping technique for residual vibration suppression in an industrial robot," *IEEE/ASME Transactions on Mechatronics*, vol. 11, no. 1, pp. 55–65, 2006.

[25] W. Tao, M. Zhang, M. Liu, and X. Yun, "Residual vibration analysis and suppression for scara robot arm in semiconductor manufacturing," in *2006 IEEE/RSJ International Conference on Intelligent Robots and Systems*. IEEE, 2006, pp. 5153–5158.

[26] N. C. Singer and W. P. Seering, "Preshaping command inputs to reduce system vibration," *Journal of dynamic systems, measurement, and control*, vol. 112, no. 1, pp. 76–82, 1990.